Nijmegen soft core *YN* potential with bound state restrictions

Dean Halderson
Physics Department, Western Michigan University, Kalamazoo, Michigan 49001
(Received 26 April 1999; published 28 October 1999)

An attempt is made to refit two sets of parameters for the Nijmegen soft core *YN* potential by including selected bound state data as well as the customary scattering data. One parameter set corresponds closely to the original Nijmegen parameters. The second is a more restricted set. It was not possible to obtain the low χ^2 values found in fits which omit the bound state restrictions. The primary difficulty is a conflict between the bound state restrictions and the ΣN scattering data. As with the original Nijmegen fit, this difficulty can be traced to the ΣN-ΛN tensor interaction. This difficulty should not adversely affect the utility of the derived potentials in hypernuclear calculations. [S0556-2813(99)03311-7]

PACS number(s): 13.75.Ev, 12.39.Pn, 21.30.−x, 21.80.+a

I. INTRODUCTION

The first extension of the Nijmegen soft core from the *NN* sector (NSC78) [1] to the strange baryon-nucleon (*YN*) sector (NSC89) [2] employed nine parameters to fit 34 cross sections and one capture ratio. Five of these parameters were form factor cutoff values whose assignments were based on the *YN* SU(3) classifications. Reasonable fits were obtained to the scattering data, and calculations of the hypertriton binding energy were surprisingly in agreement with the experimental value [3]. However, extension of the NSC89 to binding energies of heavier systems showed consistent underbinding and some spin-dependent difficulties [4–7]. Consequently, most hypernuclear calculations continued to employ the older hard core Nijmegen potential, model D [8].

A recent paper [9], based on the NSC, employed a different parameter set. In this work the form factor cutoff parameters were assigned based on the SU(3) classification of the mesons, and these parameters were the same as those used in a new *NN* fit. The parameters remaining in the *YN* fit were cutoffs for the three strange mesons, the vector magnetic $F/(F+D)$ ratio (α_M), the scalar singlet mixing angle (θ_S), and three SU(3) symmetry breaking parameters ($\lambda^S,\lambda^P,\lambda^V$), based on the $^3P_0$ model [10]. With the strange meson cutoffs held at selected values, α_M was stepped over a specified range and a fit performed at each step, yielding potentials NSC97a–f. This provided a range of parameters with different spin characteristics. These different potentials could then be used in hypernuclear calculations and the most appropriate of the potentials determined.

Some results of *g*-matrix elements and ${}^{3}_{\Lambda}$H binding energy calculations were reported in Ref. [9]. At least two of the NSC97 potentials provided very encouraging results. However, the choice of parameters in Ref. [9], unlike Ref. [2], provided predictions for the $S=-2$, -3, and -4 potentials, and the $S=-2$ results were not consistent with the reported binding energies of ${}^{6}_{\Lambda\Lambda}$He, ${}^{10}_{\Lambda\Lambda}$B, and ${}^{13}_{\Lambda\Lambda}$B.

An important result in Ref. [9] was the demonstration that many parameter sets can fit the scattering data. Therefore, the present paper takes a different approach to the construction of a universal *BB* potential from the NSC formalism. First of all, it seems quite unfair to expect *YN* potentials to have the same predictive power in bound state calculations as the *NN* potentials. Not only are the *YN* scattering data poor, but *NN* fits also include the properties of the deuteron and polarization data. The present paper presents attempts to compensate for these difficulties by incorporating selected Λ-hypernuclear binding energy results, the $\Lambda\Lambda$ contribution to double lambda hypernuclear binding energies, and the scattering data in one fit. These new data easily distinguish between versions of the NSC which provide similar fits to the scattering data.

Two modifications of the NSC89 potential with different numbers of parameters were employed. In addition, searches were made in the parameter space of the NSC97 potential. No acceptable solutions were found in this latter space. Because the assignment of cutoff parameters based on the mesons is more in keeping with the underlying Regge pole model, the NSC97 parametrization is very attractive. Therefore, a search continues in this space, and if successful results are found, they will be reported at a later date. Of the solutions obtained with modified NSC89 parameters, none could provide accurate fits to the scattering data while fitting the bound state data. The primary difficulty for the parametrizations in this paper was the inability to fit the ΣN scattering data while producing a reasonable $\Lambda\Lambda$ potential. Restriction to the regions of parameter space which provide a reasonable $\Lambda\Lambda$ potential and a fit to the bound state data produces a conflict between the $\Sigma^+ p$ and the $\Sigma^- p$ elastic cross sections and a poor value for the capture ratio at rest for stopped Σ^-. This ratio depends on the $\Sigma^- p$-$\Sigma^0 n$ and $\Sigma^- p$-Λn coupling strengths, as do the $\Sigma^- p \rightarrow \Sigma^0 n$ and $\Sigma^- p \rightarrow \Lambda n$ cross sections. However, the depths and spread of the single-particle energy levels of Λ hypernuclei also depend on the $\Sigma^- p$-Λn strength. These constraints drive the calculated capture ratio to approximately 10% below the experimental value. Attempts to reconcile the ΣN problem produced an ill-behaved $\Lambda\Lambda$ potential.

One cannot say that the NSC formalism does not contain a solution which can fit both the bound and scattering data. Although a number of parameter choices were explored in addition to those reported here, many other possible sets, including those which break SU(3) symmetry, exist. Also, the parameter space, filled with many local minima, is a very difficult one to search. One has no guarantee that solutions

TABLE I. Potential parameters. Entries with asterisks were held fixed.

Potential	α_M	α_E	ψ_D	M_{K**}	θ_S	$g_8{}^D$	α_P
NSC89	0.275	1.000*	15.00	307.81*	49.105	0.443722*	0.355
Ia	0.41042	1.000*	0.998	307.81*	46.114	0.443722*	0.355*
Ib	0.41542	1.000*	1.600	307.81*	46.114	0*	0.355*
IIa	0.47541	0.85879	11.483	679.974	42.718	0.443722*	0.355*
IIb	0.51350	0.77683	15.487	669.462	41.971	0.443722*	0.355*

do not exist, since it is not possible to ensure a global minimum. However, at this stage of the investigation, with these parameters, it appears that the condition for a good fit to the scattering data must be relaxed to provide a *YN* potential that can be carried successfully to the bound state sector. The potentials described in the body of this paper should be good candidates for these bound state calculations.

II. PARAMETERS

The failure of NSC89 to reproduce hypernuclear properties was particularly disconcerting, given that the *NN* results seemed so encouraging. The philosophy of NSC78 was to consider the mesons as members of Regge trajectories and then to isolate the contributions of the lowest occurring member in the method of Khuri [11] and Chew and Jones [12,13]. This changes the radial dependence and adds a form factor to the static one-meson exchange potential. Chew [14] has shown that, to a rough approximation, the form factor cutoff is proportional to the slope of the Regge trajectory. The NSC78 *NN* potential had only one form factor cutoff. This seems amazingly simple and conjures up textbook images of parallel lines representing the Regge trajectories. The NSC89 potential was, therefore, disappointing on two accounts: one, the poor hypernuclear results, and two, the loss of simplicity due to the use of five cutoff values.

It was because of its simplicity that the NSC potential was chosen for this investigation. The hope was that the need for few cutoff parameters would mean more predictive power for those channels not included in the fit. In an effort to retain some of this simplicity, two calculations were performed: one with parameters corresponding closely to the NSC89 set and one with a more restricted parameter set. These are listed in Tables I and II. If a potential parameter is not listed, it assumes the NSC89 value. An explanation of the parameters and their theoretical basis is contained in Refs. [1–3]. Set 1 is identical to the NSC89 parameter set, except for three changes. One, the SU(2) symmetry breaking cutoff, $\Lambda_{10'}$ is eliminated. Any required SU(2) symmetry breaking in the cutoff parameters will be considered a failure of the model. Two, one additional cutoff Λ_1 is allowed in the $S=-2$ sector. Three, the pseudoscalar $F/(F+D)$ ratio α_P is held fixed at a value of 0.355, the value obtained in NSC89. One, therefore, has eight parameters, a fit for which yielded potential Ia. For potential Ib, the octet coupling constant for the diffractive mesons, $g^D{}_8$, was set equal to zero, the NSC97 value.

Parameter set 2 was constructed so as to differ little from the *NN* potential. It retains the NSC78 *NN* cutoff value in all $S=-1$ channels, but allows a different cutoff for the $S=-2$ sector. The pseudoscalar $F/(F+D)$ ratio is again held fixed at 0.355. The magnetic $F/(F+D)$ ratio α_M, the scalar singlet mixing angle θ_S, the diffractive meson mixing parameter ψ_D, the mass of the $J=0$ component of the K^{**}, and the vector electric $F/(F+D)$ ratio α_E comprise the remaining parameters for a total of 6. Modest variations of α_E and α_M could be accommodated in a refit of the *NN* data.

III. BOUND STATE DATA

The bound state data included in these fits are the binding energies of the hypertriton, the 0^+ and 1^+ states of ${}^4_\Lambda$H, the ground state of ${}^5_\Lambda$He, the $\frac{1}{2}^+$, $\frac{3}{2}^-$, and $\frac{1}{2}^-$ single particle energies of ${}^{17}_\Lambda$O. It would be much too time consuming to perform Faddeev or variational Monte Carlo calculations for the light systems at each iteration of the fit. However, these calculations have been completed for the NSC89 [3,15], and it is necessary only to perform first-order, coupled-baryon-channel, Brueckner calculations. The channel coupling dynamics, whose importance was emphasized by other authors [16,17], will then be included. Although a first-order Brueckner calculation for $A=3$ and 4 systems will not provide accurate absolute values, binding energy differences, calculated between two potentials, will be very nearly those calculated with accurate techniques. This was shown in early calcula-

TABLE II. Momentum cutoff parameters in MeV. Entries with asterisks were held fixed.

Potential	Λ_{27}	Λ_{10}	$\Lambda_{10'}$	Λ_{27+8s}	Λ_{10*+8a}	Λ_r
NSC89	1020.00	1230.00	1270.50	820.00	1270.50	
Ia	948.040	1037.122		987.883	1037.122	862.511
Ib	916.165	1246.714		965.383	1049.309	862.042
IIa	964.53*	964.53*		964.53*	964.53*	846.346
IIb	964.53*	964.53*		964.53*	964.53*	856.058

TABLE III. Bound state parameters.

	$\hbar\Omega$ (MeV)	ω (MeV)	Δ (MeV)
${}^{3}_{\Lambda}$H	11.49	−2.37	$-0.06\hbar\Omega_\Lambda$
${}^{4}_{\Lambda}$H	11.61	−9.50	0
${}^{5}_{\Lambda}$He	12.51	Self-consistent	0
${}^{17}_{\Lambda}$O$(1/2^+)$	12.93	Self-consistent	−0.90
${}^{17}_{\Lambda}$O$(1/2^-,3/2^-)$	12.93	Self-consistent	−1.93
${}^{18}_{\Lambda\Lambda}$O	12.93	−10.00	0

tions which compared the Hamada-Johnston potential with the Reid potentials. The calculations of Refs. [3,15] provide the necessary benchmarks.

A $Q/(\omega-\frac{1}{2}E_{NL}-T_r-\Delta mc^2)$ approximation to the *QTQ* propagator is employed in all Brueckner calculations. Here E_{NL} is a diagonal center of mass kinetic energy, $\hbar\Omega(2N+L+3/2)$, T_r is a diagonal relative kinetic energy operator, and Δmc^2 is the mass difference between the two starting and the two intermediate baryons. For ${}^{3}_{\Lambda}$H, ${}^{4}_{\Lambda}$H(0^+), and ${}^{4}_{\Lambda}$H(1^+), $0\hbar\Omega$ calculations are performed. Pauli corrections are made in a one-dimensional space by

$$g=g_r/[1+g_r/(\omega-0.75(\hbar\Omega+\hbar\Omega_\Lambda))], \tag{3.1}$$

where $\hbar\Omega_\Lambda=(M_N/M_\Lambda)\hbar\Omega$. The individual single-particle energies are given by

$$\epsilon=3/2g_0+1/2g_1+3/4\hbar\Omega_\Lambda+\Delta, \tag{3.2a}$$

$$\epsilon=3/2(g_0+g_1)+3/4\hbar\Omega_\Lambda+\Delta, \tag{3.2b}$$

$$\epsilon=1/2g_0+5/2g_1+3/4\hbar\Omega_\Lambda+\Delta, \tag{3.2c}$$

for ${}^{3}_{\Lambda}$H, ${}^{4}_{\Lambda}$H(0^+), and ${}^{4}_{\Lambda}$H(1^+), respectively. In these expressions $g_I=\langle 0s(\mathbf{r})0s(\mathbf{R})S=I|g(\omega)|0s(\mathbf{r})0s(\mathbf{R})S=I\rangle$. The parameters are shown in Table III. No justification is made for these parameters, other than they reproduce NSC89 binding energies calculated by more accurate means.

More care is given to ${}^{5}_{\Lambda}$He. The binding energy is calculated in the method of Ref. [7], but with a model space limited to $2\hbar\Omega$ and Pauli corrections performed in the two-body, relative center of mass system by the average-angle technique, where $Q=0$ for $2n+2N+l+L\leqslant N_m$, $N_m=1$. The $\frac{1}{2}^+$, $\frac{3}{2}^-$, and $\frac{1}{2}^-$ single-particle energies of ${}^{17}_{\Lambda}$O were calculated in a similar fashion with $N_m=2$. Again, this procedure is fast, but crude, and a term, Δ, must be added to the standard single-particle expressions:

$$\epsilon=\langle\Delta|T|\Lambda\rangle+\sum_N\langle\Lambda N|g(\omega=\epsilon_\Lambda+\epsilon_N)|\Lambda N\rangle+\Delta. \tag{3.3}$$

A benchmark calculation for the ${}^{17}_{\Lambda}$O energies was provided in Ref. [7] where translationally invariant, self-consistent Brueckner calculations were performed in a large model space. It should be remarked that the calculations for ${}^{5}_{\Lambda}$He in Refs. [15,7] agree to within the accuracy of the calculations, so one has continuity between the two procedures.

The inclusion of ${}^{3}_{\Lambda}$H, ${}^{4}_{\Lambda}$H(0^+), ${}^{4}_{\Lambda}$H(1^+), and ${}^{5}_{\Lambda}$He will provide sensitivity to the $\boldsymbol{\sigma}\cdot\boldsymbol{\sigma}$ and tensor interactions. The inclusion of ${}^{17}_{\Lambda}$O $\frac{1}{2}^-$ and $\frac{3}{2}^-$ will provide sensitivity to the spin-orbit interaction. And, surprisingly, the depth and spread of the ${}^{17}_{\Lambda}$O single-particle energies will be a measure of the ΣN-ΛN coupling strength [7].

The $\Lambda\Lambda$ strength is estimated by calculating the ${}^1S_0$, $\Lambda\Lambda$ *g*-matrix element with a Pauli operator corresponding to ${}^{18}_{\Lambda\Lambda}$O. Again, the model space was restricted to $2\hbar\Omega$, and Pauli corrections performed in the relative center of mass basis. A value of −3.0 MeV was sought in the fit. This value should be reasonably consistent with 4.0–4.5 MeV of binding in ${}^{6}_{\Lambda\Lambda}$He, if one assumes mild Pauli corrections. Inclusion of this matrix element is a much tighter restriction than one would think. Since it involves solving the $\Lambda\Lambda$, $\Sigma\Sigma$, and ΞN coupled channel problem, it is demanding well-behaved potentials in all channels. Without this restriction, fits to the scattering data and Λ hypernuclei improve significantly.

Taking this $\Lambda\Lambda$ *g*-matrix element to be the contribution of the $\Lambda\Lambda$ interaction in the *p* shell is the worst of the approximations. Many of the $\Lambda\Lambda$ potentials that are generated in parameter fits are very ill behaved. Therefore, one does not know if the *g*-matrix element at a particular search point is calculated accurately. Also, even when the $\Lambda\Lambda$ potential is reasonably smooth, the convergence of the $Q-1$ corrections can be very poor for some potentials, and the limited space employed in this approximation is not adequate. However, the inclusion of this *g*-matrix element will eliminate the very large fraction of the parameter sets which give unreasonable values for the $\Lambda\Lambda$ contribution to $\Lambda\Lambda$ hypernuclei.

The bound state data are entered as shown in Table IV. The quantities in curly brackets are not experimental uncertainties, but are the uncertainty values read into the search

TABLE IV. $-B_\Lambda$ (MeV).

	Expt.	Potential Ia	Potential Ib	Potential IIa	Potential IIb
${}^{3}_{\Lambda}$H	−0.13 {0.01}	−0.18	−0.20	−0.22	−0.17
${}^{4}_{\Lambda}$H(0^+)	−2.20 {0.03}	−2.11	−2.15	−2.17	−2.21
${}^{4}_{\Lambda}$H(1^+)	−1.15 {0.03}	−1.13	−1.15	−1.24	−1.47
${}^{5}_{\Lambda}$He	−3.10 {0.04}	−1.65	−1.61	−1.68	−1.85
${}^{17}_{\Lambda}$O$(1/2^+)$	−13.60 {0.03}	−13.84	−13.82	−13.78	−13.74
${}^{17}_{\Lambda}$O$(3/2^-)$	−2.95 {0.06}	−3.10	−3.03	−3.08	−3.11
${}^{17}_{\Lambda}$O$(1/2^-)$	−2.05 {0.06}	−2.19	−2.09	−2.15	−2.14

TABLE V. Scattering χ^2 values.

Reaction	Potential Ia	Potential Ib	Potential IIa	Potential IIb
$\Sigma^+p\to\Sigma^+p$	0.6	0.3	14.3	16.2
$\Sigma^-p\to\Sigma^-p$	2.3	2.1	13.0	9.2
$\Sigma^-p\to\Sigma^0n$	9.5	6.9	8.3	7.4
$\Sigma^-p\to\Lambda n$	9.4	8.1	5.4	5.3
$\Lambda p\to\Lambda p$	4.0	4.2	5.1	7.5
Subtotal	25.8	21.6	46.1	45.6
r_C	25.1	11.7	41.0	33.6
Total	50.9	33.3	87.1	79.2

code which force a good fit to the bound state data. A χ^2, based on these fictitious uncertainties, would be a measure of the goodness of fit to these data.

IV. RESULTS

Several fits of equal quality were obtained with parameter set II. The results of two of these fits are reported in this paper as potential IIa and potential IIb. These two fits, plus the potential I fits, span a reasonably large range of α_M. The χ^2 values for the cross sections plus capture ratio are shown in Table V. The total cross sections plus capture ratio χ^2 should be compared to the values near 16 obtained in Refs. [2,9]. For potentials I and II approximately one-third to one-half of the χ^2 comes the capture ratio alone. In Refs. [2, 9] the contribution of the capture ratio was negligible. The experimental value for the capture ratio is 0.468 ± 0.010. The results for potentials Ia, Ib, IIa, and IIb are 0.418, 0.434, 0.404, and 0.410, respectively. All fits which included the bound state restrictions produced a capture ratio which was too small. If a fit was forced to reproduce the capture ratio, most of the Λ hypernuclei became too deeply bound.

The $S=-1$ cutoff parameter Λ_1 had the greatest effect on the overall χ^2. By allowing it to vary, one obtains many acceptable fits for both parameter sets I and II. Potential II exhibited a nice feature in this regard, in that the $\Lambda\Lambda$ g-matrix element goes nearly linearly with Λ_1. The other parameters have a more modest effect, in that a chosen parameter can be fixed at some reasonable value and the other parameters adjusted so that the increase in the overall χ^2 is not large. In this sense, α_E and $M_{K^{**}}$ are as important as the other parameters in parameter set II. By allowing $M_{K^{**}}$ to vary, one is providing some flexibility in the $S=-1$ exchange potential. This can also be accomplished by allowing the cutoff parameter for the K or K^* to vary. In fact, adding K and K^* cutoff parameters improves the fit. However, other choices for additional cutoffs, such as those of potential I, also improve the fit. Since the rationale behind parameter set II was that it be simple, the number of parameters was held at 6.

The NSC89 parameter values have been included in Tables I and II for comparison. The NSC89 and potential I cutoffs do not appear to be correlated. In fact, no acceptable solutions were found when the NSC89 parameter values were allowed to vary by 10%. A significant difference is apparent in α_M and ψ_D. All solutions have a preference for α_M values larger that the NSC89 value of 0.275. The results of 0.410 42 and 0.415 42 for potentials Ia and Ib are quite close to the static SU(6) value of 2/5. The value of ψ_D controls the $F/(F+D)$ ratio α_D for the diffractive mesons. The NSC89 value of $\psi_D=15°$ gives $\alpha_D=0.9984$, while the potentials Ia, IIa, and IIb have $\alpha_D=0.2993$, 0.8256, and 1.0221, respectively. The ΛNK^{**} coupling constant is given by

$$g^D{}_{\Lambda NK^{**}}=-g_8{}^D(1+2\alpha_D)/\sqrt{3}, \tag{4.1}$$

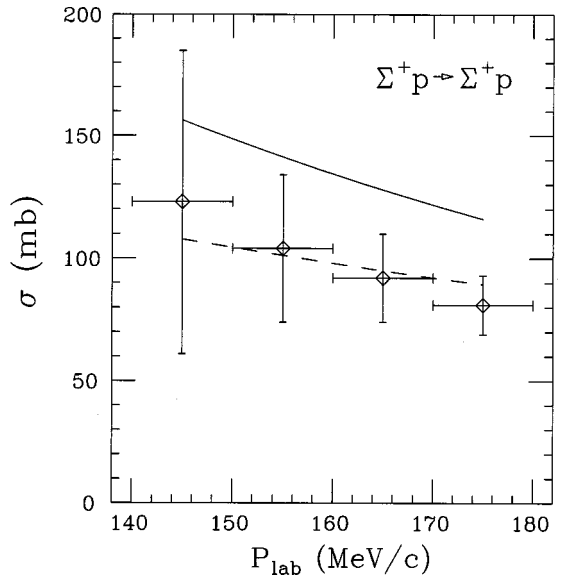

FIG. 1. The dashed line represents the Σ^+p integrated cross section results for potential Ia. The solid line is for potential IIa. Data are from Ref. [20].

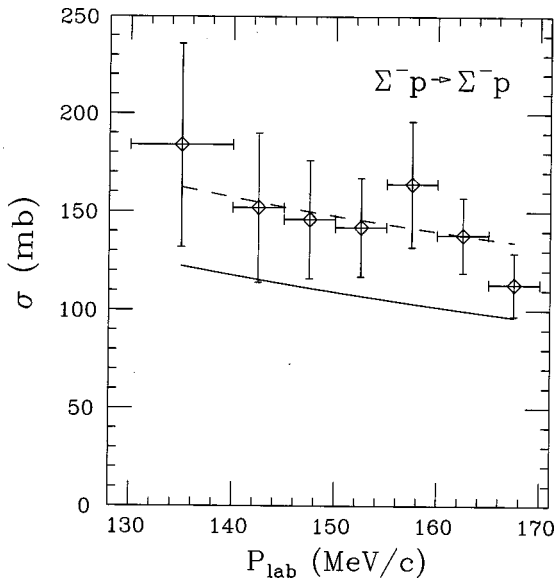

FIG. 2. The dashed line represents the Σ^-p integrated cross section results for potential Ia. The solid line is for potential IIa. Data are from Ref. [20].

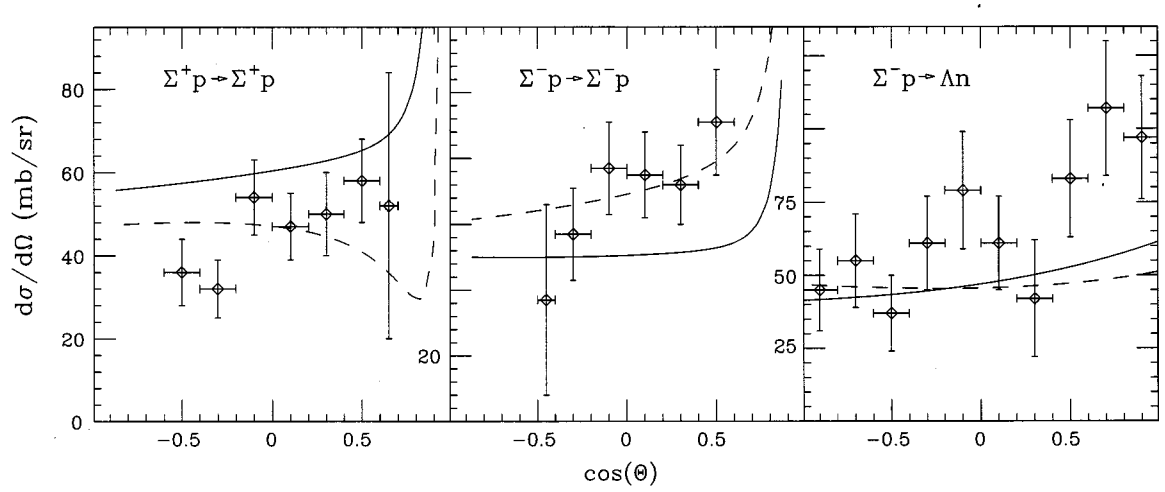

FIG. 3. The dashed line in the first panel represents the $\Sigma^+ p$ differential cross section results for potential Ia at $p_{\rm lab}=170$ MeV/c. The solid line is for potential IIa. Data are from Ref. [20]. The dashed line in the second panel represents the $\Sigma^- p$ differential cross section results for potential Ia at $p_{\rm lab}=160$ MeV/c. The solid line is for potential IIa. Data are from Ref. [20]. The dashed line in the third panel represents the $\Sigma^- p \rightarrow \Lambda n$ cross differential cross section results for potential Ia at $p_{\rm lab}=160$ MeV/c. The solid line is for potential IIa. Data are from Ref. [21].

where ${g_8}^D = g_{A_2 NN}$ is the octet coupling constant. Solutions for parameter set II, which allowed variation of M_{K**}, seek large values of α_D, which give large values of ${g^D}_{\Lambda NK**}$. Parameter set I, for which M_{K**} was fixed, sought a small value of α_D, which gives a small value of ${g^D}_{\Lambda NK**}$. In fact, in NSC97, ${g_8}^D$ was set equal to zero, and flexibility in the exchange potential was provided by separate cutoffs for K and K^*. This preference for a small ${g^D}_{\Lambda NK**}$ was the motivation for setting ${g_8}^D$ equal to zero for potential Ib, and a significant improvement in the capture ratio was produced.

All reasonable fits for potential II result in values M_{K**} which are larger than the 307 MeV used in NSC89. Typically, the values sought are between 550 and 700 MeV. This may be providing some clue as to the importance of the missing two-meson exchange terms in the potential. The lightest two-meson exchange in the strangeness exchange channel would be π plus K. Although with no pole terms the diffractive meson potentials would not have the correct radial behavior, they may provide the necessary massaging of the other potentials in the two-meson exchange range. Other comments on the role of possible two-meson exchange contributions may be found in Refs. [18,19].

The cross sections for potential Ia (dashed lines) and IIa (solid lines) are plotted in Figs. 1–6. The results for potentials Ib and IIb are very similar to those of potentials Ia and IIa. A comparison of Figs. 1 and 2 clearly indicates the conflict between $\Sigma^+ p \rightarrow \Sigma^+ p$ total cross section and the $\Sigma^- p \rightarrow \Sigma^- p$ total cross section for potential II. An accurate fit to $\Sigma^- p$ produces a $\Sigma^+ p$ which is too large. The results in Figs. 1 and 2 represent a compromise between the two cross sections. This conflict was ameliorated in NSC89 by including different cutoffs in the $T=3/2$ ΣN channel for $\Sigma^- p$ and

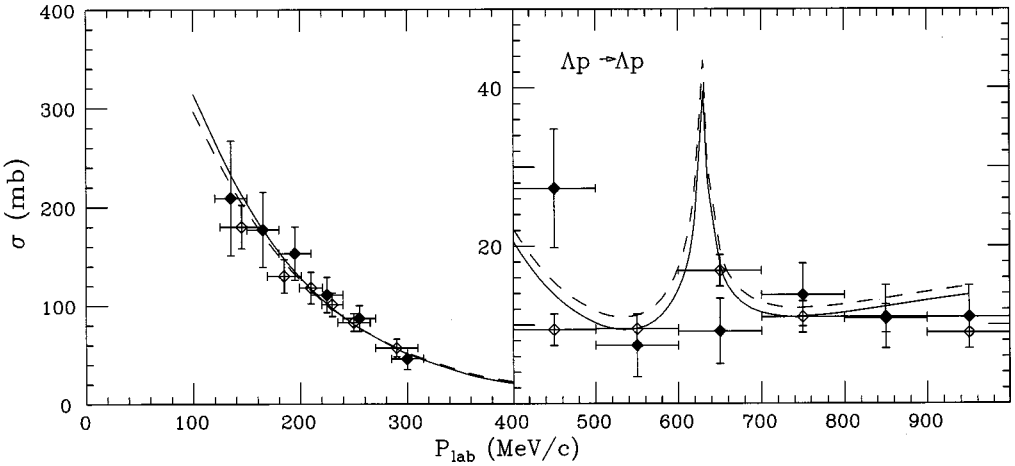

FIG. 4. The dashed lines represent the Λp integrated cross section results for potential Ia. The solid lines are for potential IIa. The open diamonds in the first panel are data from Ref. [22] and the solid diamonds are from Ref. [23]. The open diamonds in the second panel are data from Ref. [24] and the solid diamonds are from Ref. [25].

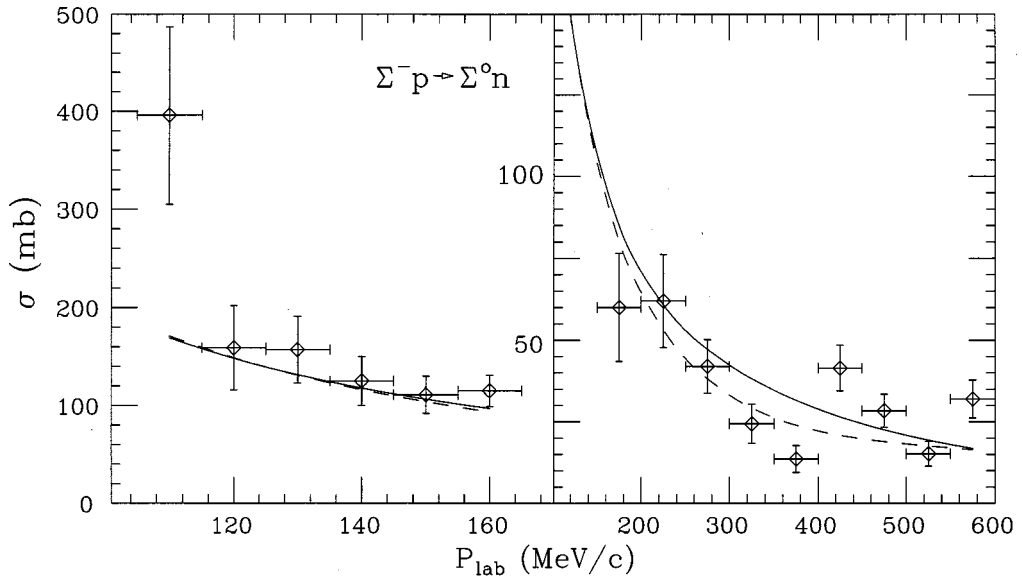

FIG. 5. The dashed lines represent the $\Sigma^- p \to \Sigma^0 n$ total cross section results for potential Ia. The solid lines are for potential IIa. Data in the first panel are from Ref. [21]. Data in the second panel are from Ref. [26].

$\Sigma^+ p$. As mentioned above, SU(2) symmetry breaking in the cutoff values is not allowed in this work. The angular distributions in Fig. 3 show the same effect as the total cross sections in these channels. One should also note in Fig. 3 that, although potential I fits the $\Sigma^- p$ and $\Sigma^+ p$ integrated elastic cross sections, it may be demonstrating some difficulty with the Coulomb-nuclear interference in $\Sigma^+ p$.

Fits to the other total cross sections are similar for both potentials I and II, and the fits are generally good. The high energy data in the second panels of Figs. 4, 5, and 6 were not included in the fit, but are well represented by all potentials. Figure 7 shows the recent data of Ref. [19] for higher energy $\Sigma^+ p \to \Sigma^+ p$. Although the error bars are large, these data may be regarded as another test of the predictions of the potentials. The results of potential Ia (dashed line) are outside of the error bars, while those of potential Ib (dot-dashed line) fall within, but at the top of the error bars, much like the original NSC89. The results of potentials IIa and IIb are nearly identical (solid line), and they provide a better fit to these data.

A possible exception to the claim of generally good fits is the $\Sigma^- p \to \Lambda n$ cross section at low energies. The calculated cross sections appear to be rising too fast as the momentum decreases. This would be the most likely source of difficulty with the capture ratio, since the capture ratio is given by the zero-energy cross section ratios

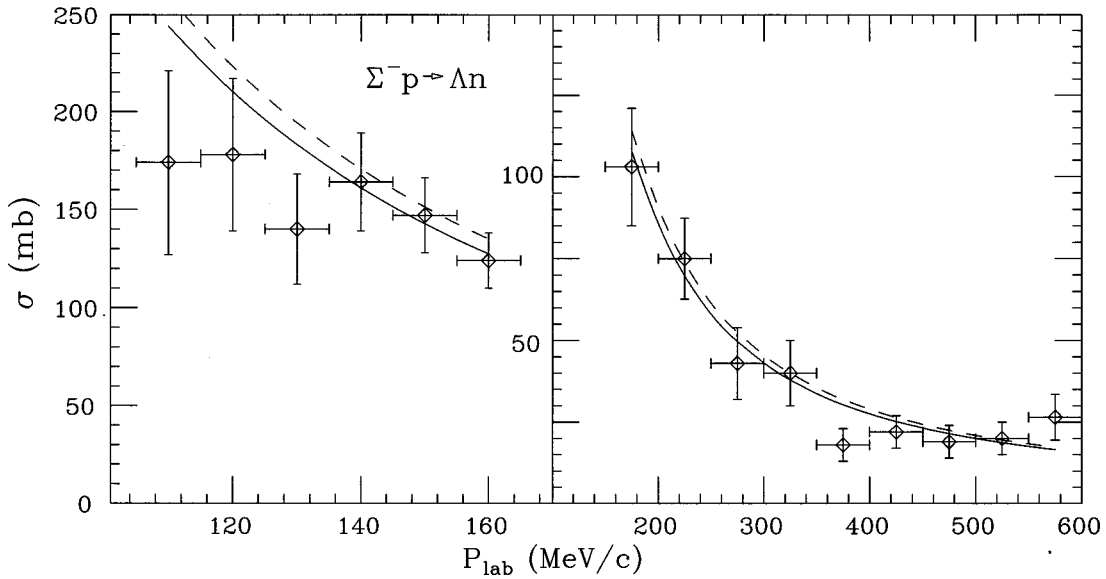

FIG. 6. The dashed line represents the $\Sigma^- p \to \Lambda n$ total cross section results for potential Ia. The solid line is for potential IIa. Data in the first panel are from Ref. [21]. The data in the second panel are from Ref. [26].

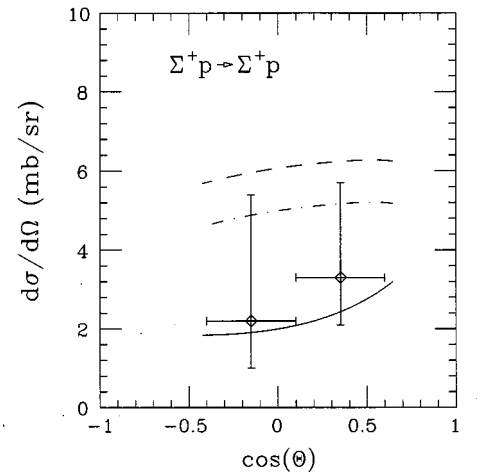

FIG. 7. The dashed line represents the $\Sigma^+ p$ differential cross section results for potential Ia at $p_{\rm lab}=400$ MeV/c. The solid line is for potential IIa. The dot-dashed line is for potential Ib. Data are from Ref. [27].

$$r_C=\frac{1}{4}\frac{\sigma_s(\Sigma^- p\to\Sigma^0 n)}{\sigma_s(\Sigma^- p\to\Lambda n)+\sigma_s(\Sigma^- p\to\Sigma^0 n)} + \frac{3}{4}\frac{\sigma_t(\Sigma^- p\to\Sigma^0 n)}{\sigma_t(\Sigma^- p\to\Lambda n)+\sigma_t(\Sigma^- p\to\Sigma^0 n)}. \quad (4.2)$$

A large low energy cross section for $\Sigma^- p\to\Lambda n$ produces a small capture ratio.

The bound state results are shown in Table IV. In this table one can see that ${}^{5}_{\Lambda}$He is underbound for all potentials. The source of this underbinding is the strong ΣN-ΛN tensor force. This is the inverse of the old ${}^{5}_{\Lambda}$He binding problem, where a central potential which fits the binding energy of ${}^{3}_{\Lambda}$H and ${}^{4}_{\Lambda}$H will overbind ${}^{5}_{\Lambda}$He. This problem with the ΣN-ΛN tensor force relates directly to the capture ratio problem. A large fraction of the $\Sigma^- p\to\Lambda n$ cross section is due to the tensor force. This is the reason one can have a total cross section which is too large at small energies and at the same time have good fits to the binding energy of ${}^{3}_{\Lambda}$H and ${}^{4}_{\Lambda}$H. Tensor forces generally have less effect on binding than on scattering [15]. The connection between the $\Sigma^- p\to\Lambda n$ cross and the ${}^{5}_{\Lambda}$He binding is evident when a fit is forced to the ${}^{5}_{\Lambda}$He binding energy. Then the capture ratio comes very close to the experimental value.

Therefore, potentials I and II, just like NSC89 [15], rely too heavily on the contribution of this strong tensor force to produce observed binding energies and cross section magnitudes. It was hoped that a refit of the potential parameters would alleviate this difficulty. However, the NSC, at least for the parameter sets in this paper, does not produce potentials with the forms necessary to move the strength from the tensor to central potential and still provide a fit to both the bound state and scattering data.

V. CONCLUSION

The primary purpose of this paper was to produce a version of the NSC which would be faithful to the original model, yet be useful in hypernuclear calculations. Four potentials, derived from two parameter sets, were developed by fitting to selected bound state data in addition to the capture and scattering data. The addition of the bound states doubles, at best, the scattering plus capture ratio χ^2. This was due primarily to the inability to reduce the dependence on the strong ΣN-ΛN tensor force.

Two main points emerge from this investigation. First, until polarization or analyzing power data are available, one should consider some bound state data in the development of a potential. Otherwise, the number of possible solutions becomes too large. In that case it becomes a matter of chance whether one picks the solution with the correct spin dependence or with a reasonable extension into the $S=-2$ sector. In addition, a fit to only scattering data relies on data sets which may well have systematic errors. One is reminded of the discrepancy encountered when comparing $\Sigma^- p\to\Lambda n$ total cross sections [23] with $\Lambda p\to\Sigma^0 p$ [25] via detailed balance and isospin [28].

Second, the development of these potentials is a continuing process, and the results in this paper represent just one step. The next step, the one for which the potentials were designed, is to carry them into the bound state sector and investigate their predictions in a number of hypernuclear calculations. During these calculations, it would be very useful to look for observables which are sensitive to the strong ΣN-ΛN tensor interaction. It will also be useful to determine whether potentials I and II have different bound state predictions, and hence determine the sensitivity to potential characteristics. This information will assist in the next iteration of the search for a universal *BB* interaction.

ACKNOWLEDGMENTS

Thanks are due to V. G. J. Stoks for providing the potential code for the Nijmegen soft core. This work was supported by the National Science Foundation under Grant No. PHY-9732634.

[1] M. M. Nagels, T. A. Rijken, and J. J. de Swart, Phys. Rev. D **17**, 768 (1978).
[2] P. M. M. Maessen, Th. A. Rijken, and J. J. de Swart, Phys. Rev. C **40**, 2226 (1989).
[3] K. Miyagawa and W. Glockle, Nucl. Phys. **A585**, 169c (1995).
[4] Y. Yamamoto and H. Bando, Prog. Theor. Phys. **83**, 254 (1990).
[5] T. Motoba and Y. Yamamoto, Nucl. Phys. **A585**, 29c (1995).
[6] T. Hasegawa *et al.*, Phys. Rev. Lett. **74**, 224 (1995).
[7] D. Halderson, Phys. Rev. C **48**, 581 (1993).
[8] M. M. Nagels, T. A. Rijken, and J. J. de Swart, Phys. Rev. D **12**, 744 (1975); **15**, 2547 (1977).
[9] Th. A. Rijken, V. G. J. Stoks, and Y. Yamamoto, Phys. Rev. C **59**, 21 (1999).

[10] L. Mieu, Nucl. Phys. **B10**, 521 (1969); R. Carlitz and M. Kislinger, Phys. Rev. D **2**, 336 (1970).
[11] N. N. Khuri, Phys. Rev. **130**, 429 (1963).
[12] G. F. Chew and C. E. Jones, Phys. Rev. **135**, B208 (1964).
[13] G. F. Chew, Phys. Rev. **140**, B1427 (1965).
[14] G. F. Chew, Prog. Theor. Phys. Suppl. **Ext. No.,** 118 (1965).
[15] J. A. Carlson, in LAMPF Workshop on (π,K) Physics, edited by B. F. Gibson, W. R. Gibbs, and M. B. Johnson, AIP Conf. Proc. No. 224 (AIP, New York, 1991), p. 198.
[16] S. B. Carr, I. R. Afnan, and B. F. Gibson, Nucl. Phys. **A585**, 315c (1995).
[17] Y. Yamamoto and H. Bando, Prog. Theor. Phys. Suppl. **81**, 9 (1985).
[18] V. G. J. Stoks and Th. A. Rijken, Phys. Rev. C **59**, 3009 (1999).
[19] Th. A. Rijken, Nucl. Phys. **A639**, 29c (1998).
[20] F. Eisele, H. Filthuth, W. Fölisch, V. Hepp, E. Leitner, and G. Zech, Nucl. Phys. **B37**, 204 (1971).
[21] R. Engelmann, H. Filthuth, V. Hepp, and E. Kluge, Phys. Lett. **21**, 587 (1966).
[22] G. Alexander, U. Karshon, A. Shapira, G. Yekutieli, R. Engelmann, H. Filthuth, and W. Lughofer, Phys. Rev. **173**, 1452 (1968).
[23] B. Sechi-Zorn, B. Kehoe, J. Twitty, and R. A. Burnstein, Phys. Rev. **175**, 1735 (1968).
[24] J. A. Kadyk, G. Alexander, J. H. Chan, P. Gaposchkin, and G. H. Trilling, Nucl. Phys. **B27**, 13 (1971).
[25] M. Hauptman, J. A. Kadijk, and G. H. Trilling, Nucl. Phys. **B125**, 29 (1977).
[26] D. Stephen, Ph.D. thesis, University of Massachusetts, 1970.
[27] J. K. Ahn *et al.*, Nucl. Phys. **A648**, 263 (1999).
[28] G. Alexander, H. H. Hall, N. Jew, G. Kalmus, and A. Kernan, Phys. Rev. Lett. **22**, 483 (1969).